Korean J. Chem. Eng., 39(4), 838-852 (2022)
DOI: 10.1007/s11814-021-1002-2

pISSN: 0256-1115
eISSN: 1975-7220

Dynamic analysis of a flare network: Gas blow-by and depressurization system

Yeonpyeong Jo*, Dongjun Lee*, Baasanjargal Sukhbold*, Youngtak Jo, and Sungwon Hwang*,**,†**

*Department of Chemistry and Chemical Engineering, Inha University, Incheon 22212, Korea
**Department of Smart Digital Engineering, Inha University, Incheon 22212, Korea
(*Received 9 July 2021 • Revised 2 October 2021 • Accepted 31 October 2021*)

Abstract−Flare network systems are essential in chemical plants to ensure process safety. In particular, the flare network system of offshore platforms is expected to play a critical role, mainly due to the isolated location from the onshore safety infrastructure and the compact structure of the platforms. However, owing to the spatial and weight limitations of the offshore platforms, it is important to reduce the pipe sizes used in the flare network, while also satisfying the installation codes and standards for such systems. In this study, flare network systems of the offshore platforms were designed and optimized based on dynamic simulation results. For this, two separate cases of "control valve fail-open" and "depressuring system" were considered. In the former scenario, we observed 'gas blow-by' due to the inlet of high-pressure gas into the low-pressure separator, caused by liquid disappearance in the high-pressure separator. Under the latter scenario, we analyzed whether the developed design of the flare networks satisfies the depressuring rate requirement from API Standard 521 and noticed potential extreme decline in temperature in a unit during the relieving condition. As a result, we developed a strategy to decrease depressuring rate in the unit. Lastly, we saved capital costs by reducing the pipe sizes based on the optimization results, obtained from the dynamic simulation analysis.

Keywords: Gas Blow-by Modeling, Control Valve Fail-open, Depressuring Process, Flare Network System Optimization

INTRODUCTION

Flare network systems are essential for ensuring process safety in various plants, including petrochemical, refinery, and offshore platforms that extract fossil fuels from the subsea region [1]. A flare network system prevents overpressure, which can lead to the explosion of units or the leakage of hazardous materials from these units, under abnormal circumstances such as fire exposure, control failure, utility failure, unexpected chemical reaction, cooling or reflux failure, and hydraulic expansion [2]. Unexpected process upsets or accidents are significantly detrimental to offshore platforms because of their distance from land and the compact configuration of the units, due to space limitations [3]. Thus, the explosion of a unit in the topside process can lead to a catastrophic disaster within a short time, as in the case of the Piper Alpha disaster, one of the most deadly accidents on offshore oil rigs [4].

Over the past few years, many studies have focused on the safety analysis and process configuration optimization of onshore and offshore platforms. These studies employed methods involving fault tree analysis and dynamic Bayesian networks [5,6], failure analysis [7], risk-based configuration optimization for the offshore topside process [8], flare tip modeling through computational fluid dynamics [9], and risk-effectiveness design for the flare height in LNG plants [10]. Additionally, flare gas combustion mitigation methods, such as flare gas recovery methods [11,12] and the integration of flare gas with a fuel gas supply system [13,14], have been actively examined. However, based on our investigation, few studies have focused on optimizing the flare network system.

Generally, a flare network system has 1) pressure safety valves (PSVs) that are installed on the process units, 2) tailpipes that connect the PSVs to the sub/main headers, 3) main headers that gather the transported flare loads from the tailpipes, 4) a knock-out (KO) drum that separates the flare loads into the vapor and liquid phases, and 5) flare stacks in which the vapor from the KO drum is burned. The configuration of the typical flare network system is shown in Fig. 1. The flare network system is generally designed based on the steady-state condition by using pre-estimated relieving conditions, and the steady-state model focuses only on the flare network system. Therefore, changes in the relieving conditions over time, as governed by the process conditions, cannot be considered. Additionally, the steady-state model-based design of the flare network systems leads to an overestimation of the pipeline size. This, in turn, leads to capital cost increase and limited spatial availability on offshore platforms [15]. However, the size of the pipeline can be minimized via dynamic simulations by considering the regulations and requirements from the API Standard and the NORSOK Standard [16], as demonstrated in our previous study [17].

As discussed, to the best of our knowledge, few studies have dynamically analyzed the flare network system and optimized the pipeline size considering an unpredicted emergency in the main process. Davoudi et al. [18] conducted pipeline sizing based on the pool fire scenario for the high-pressure (HP) process in the refinery plants of South Pars, by using an Aspen Flare System Analyzer (AFSA), which is a steady-state model. They considered the Mach number (Ma), the backpressure, and ρv^2 to size the HP sub-header and assessed the acceptability of the designed pipe diameter of 40 in. The results revealed that the originally designed diameter of the HP sub-header satisfied the regulations of the API Standard. How-

†To whom correspondence should be addressed.
E-mail: sungwon.hwang@inha.ac.kr

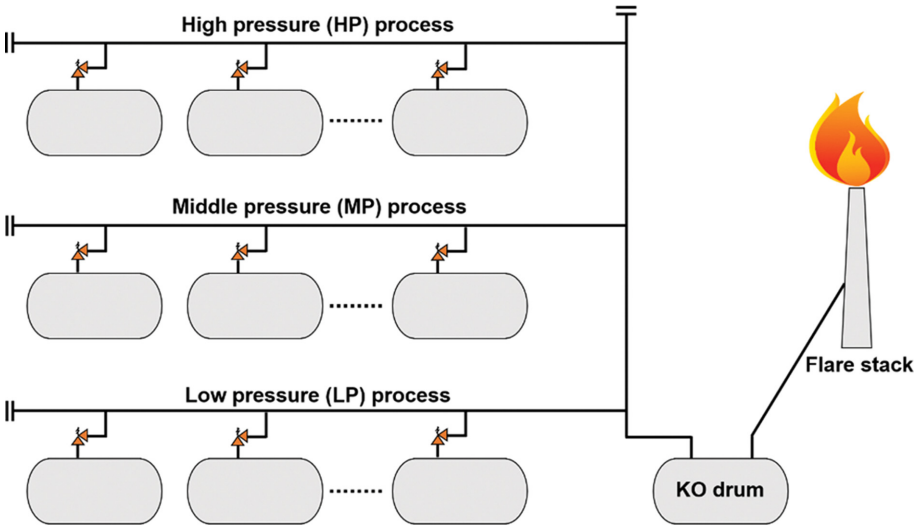

Fig. 1. Schematic of a general flare network system.

ever, they did not optimize the HP sub-header, although the calculated values of the variables, i.e., Ma of 0.3073 (43% of regulations), backpressure of 11.8 barg (84% of regulations), and ρv^2 of 60,668 kg/(m s^2) (40% of regulation), were less than those prescribed in the regulations.

Pemii et al. [19], by using the concept of pinch analysis, optimized the pipeline size considering the integration of the gas flare network systems from two different plants. Given that pinch technology has been proven to be an effective process optimization method [20], they considered pinch technology for linear programming optimization. They employed Ma, backpressure, noise, and ρv^2 as the optimization constraints. They set the maximum value of Ma as 0.5 and 0.7 for the header and tailpipes, respectively; a backpressure of 10% of the PSV's set pressure; noise levels of 80 dB and 115 dB for the upstream and downstream of the source, respectively; and ρv^2 of 6,000 kg/(m s^2). The optimization results revealed that the pipeline diameters for the integrated flare network could be reduced by 20% via pinch analysis compared to the original integrated model.

Somozas et al. [21] considered the debottlenecking potential of a flare network system for an emergency depressuring process via dynamic simulations for three different offshore platforms. They conducted simulations of a full-scale process depressuring system and determined that the maximum mass flow rate for facility A (smallest-scale process), B (middle-scale process), and C (largest-scale process) was reduced by 13.0%, 13.5%, and 24.3%, respectively, when compared to that in the steady-state simulation. The results indicated that the debottlenecking potential increases with the process scale. They also suggested the potential benefits of developing a highly complex model for obtaining more realistic behaviors when designing the flare network system, as compared to those obtained when designing each process unit alone.

Dynamic analyses of the depressing/blowdown process have been actively investigated and summarized in the literature [22]. Shafiq et al. [23] investigated the optimized orifice size of a blowdown valve used to prevent the solidification of the CO_2-CH_4 binary mixture owing to a rapid decrease in temperature, in the depressuring process of a cryogenic distillation column. They observed that, as the concentration of CO_2 increased, the probability of the mixture solidifying at a relatively high temperature also increased, due to the high solidification temperature of CO_2. Furthermore, they observed that, in addition to the effect of CO_2, the effect of the initial temperature and orifice size on the cryogenic mixture's solidification was significant. Based on the empirical relationship between these critical variables, they suggested a correlation to estimate the optimal orifice size as a function of the initial temperature and CO_2 concentration, and they also proposed an equation for estimating the depressurization time when the optimal orifice size is applied. Additionally, the blowdown/depressuring process for cryogenic units, which is usually used in liquefied natural gas plants, has been actively analyzed [24-26].

Ebrahimi et al. [27] emphasized that the depressuring process in the non-fire case should be analyzed to avoid vessel failures due to the low temperature caused by the high depressuring rate. Given that the depressuring process is usually designed based on the fire case, in accordance with the criteria of API Standard 521, the size of the equipment, and the blowdown valve, need to be conservatively designed. This implies an extremely low temperature during the depressuring process, especially in the cold depressuring process. The cold depressuring process might happen during blowdown period at process shutdown for regular maintenance. Ebrahimi et al. suggested that the decrease in temperature to extremely low values can be avoided by increasing the depressuring time. Furthermore, they suggested the necessary steps for the slow depressurization process, which are as follows: a) depressurization calculation for fire and cold cases; b) mechanical check and feedback for cold depressurization calculations; c) mechanical creep analysis for fire case and feedback for depressurization calculation; and d) recommendation. Based on these proposed steps, they conducted an analysis of the slow depressuring process down for an absorber. Their results indicated that the slow depressuring process can prevent vessel failure during fires and under cold depressuring scenarios.

Based on the aforementioned literature, the dynamic analysis of a pressure relief system is significantly important. Furthermore, dynamic analyses provides more practical than steady-state analyses, and they allow potential for saving capital costs. However, there is a paucity of studies on this topic, and most previous studies have so far focused on the fire scenario. Specifically, API Standard 521 clearly states that process engineers should consider the gas blow-by situation caused by control failure. Additionally, the analysis of a full-scale depressuring process under the non-fire scenario is important for preventing the failure of the process unit due to the rapid decline in temperature. Based on this, we propose a model integrating the flare network system and the main process to investigate the dynamic behavior of the system. To consider realistic responses of the main process and the flare network system during process upsets, the "inlet control valve fail-open" scenario was developed by using the dynamic model and compared with the steady-state model. In particular, the depressuring process for the low-pressure (LP) process was analyzed to evaluate the suitability of the size of the blowdown valve in an industrial offshore project. The novelty of this study is as follows: a) we developed a gas blow-by model for emergencies in offshore platforms and determined that the dynamic model shows more realistic behavior for the flare network than the steady-state model, by integrating the flare network system with the main process; b) we constructed a depressuring system and analyzed it dynamically; and c) we optimized the pipeline size of the flare network system, which, in turn, led to a minimization of the capital costs and a maximization of spatial availability.

The remainder of this paper is organized as follows. In Section 2, the scenario analysis, i.e., the inlet control valve fail-open and non-fire depressuring systems, is presented. In Section 3, the modeling methodology for the steady-state and dynamic models of the inlet control valve fail-open scenario is described; the modeling of the depressuring system is also described. Subsequently, the simulation results of the steady-state and dynamic models for the inlet control valve fail-open scenario and the depressuring system are presented in detail, and the results of the pipeline size optimization are described. Finally, we conclude by listing the advantages and importance of the integrated model and presenting the dynamic analysis of the flare network system design.

SCENARIO ANALYSIS

In this study, two scenarios for flare relieving and depressuring were considered: "inlet control valve fail-open" and "non-fire depressuring process." The equipment and operating datasets for each scenario were obtained from an actual industrial offshore project.

1. Inlet Control Valve Fail-open Scenario

Based on API Standard 521, process engineers should consider that HP vapor flows into the LP system due to the loss of liquid in the HP vessel during the control valve fail-open scenario, even if it is not the governing scenario. The inflow of HP vapor into the LP system is referred to as "gas blow-by" [2]. In the gas blow-by case, an overpressure of 110% of the maximum allowable working pressure (MAWP) is typically allowed in the LP system. Fig. 2 presents a schematic of the control valve fail-open scenario. The LP separator is connected with the HP separator developed in our previous study [17]. Therefore, the liquid hydrocarbon mixture from the HP separator flows into the LP separator. In the actual project, the liquid level and the pressure of the HP separator are controlled by the LP separator inlet control valve and the pressure controller, respectively. However, the liquid level controller is removed in this study. Thus, the scenario can be simulated by manually opening the liquid level control valve. Given that the liquid level controller is removed, an accurate valve stem position is required to maintain the liquid level in the HP separator and a constant inlet flow rate for the LP separator. Thus, the inlet control valve's stem position is obtained from the steady-state model, which satisfies the aforementioned consideration.

In this study, we assumed that the liquid level and pressure of

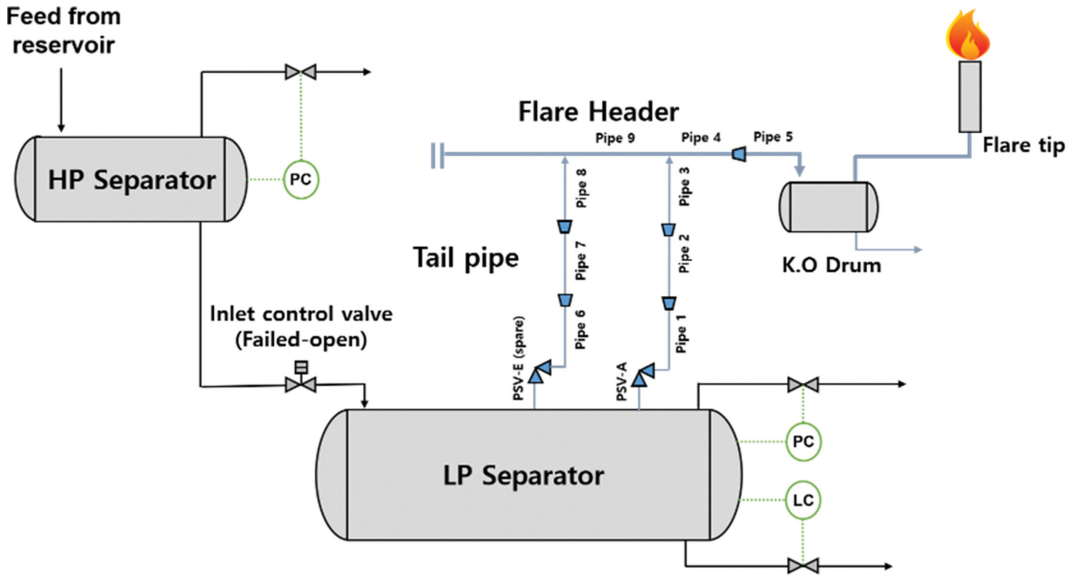

Fig. 2. Schematic of the inlet control valve fail-open scenario.

the LP separator are controlled under the normal and control valve fail-open scenarios. When the scenario commences, the inlet control valve begins to open, and it requires 10 s to open fully. Given that the HP separator is under normal operation when the scenario commences, a large amount of the liquid hydrocarbon mixture from the HP separator flows into the LP separator via the fully opened valve, while the feed flow from the reservoir continues to flow into the HP separator. Hence, the liquid level of the HP separator continuously decreases, and the liquid level in the HP separator finally reaches zero. Subsequently, gas blow-by occurs. In this study, a pressure safety valve was installed to release the overpressured gas from the LP separator, and another valve was installed as an alternative when the first valve is under maintenance.

2. Depressurization Process

The depressurization system is critical during an emergency or a planned shutdown to ensure safety during the depressurization process [26]. During the depressurization process, the unit's temperature decreases rapidly due to the rapid depressurization, and therefore, the unit can fail due to cracks in its wall, caused by the considerably low temperatures. This, in turn, leads to catastrophic consequences. In this study, the effect of depressurization under the non-fire case for the LP process in an offshore platform was analyzed dynamically. Specifically, the rates of decrease in the pressure and temperature of each unit were analyzed, and the suitability of the designed process was evaluated based on API Standard 521.

A flow chart of the depressurization process for the LP process is presented in Fig. 3. The LP system consists of nine process units and a KO drum. Similar to the inlet control valve fail-open scenario, when the depressurization process commences, the blowdown valves installed at all the units begin to open and require 10 s to open fully.

MODELING METHODOLOGY

The flowcharts for the steady-state, dynamic, and depressuring system are shown in Fig. 4. For the steady-state model, the pre-estimated relieving conditions are manually specified into the PSV model. In this study, the pre-estimated relieving conditions were obtained from the industrial project. Then, the Mach number of each pipe was automatically calculated. Next, an evaluation of the pipe size was conducted using the obtained Mach number. If the Mach number exceeds the criteria, the pipe size needs to be increased. For, dynamic model, the simulation starts with the normal operating condition. Then, the event occurs at an arbitrary point. Once the event proceeds, the relieving conditions are automatically calculated based on the process conditions change. Mach number is then calculated using a user-defined function, and optimization of pipe sized is conducted based on the obtained Mach number. For depressuring process, all of the units in the LP system start to open their BDVs at the same point. All the BDVs open fully for 10 s and the change in temperature and pressure is observed for 1 hr. Then, an evaluation of the change in pressure and temperature is conducted to make a decision whether the depressuring process is well designed or not.

1. Steady-state Modeling of the Inlet Control Valve Fail-open Scenario

Generally, a flare network system is designed under steady-state conditions. The most frequently used modeling tool is the Aspen Flare System Analyzer (AFSA). To design a flare network system

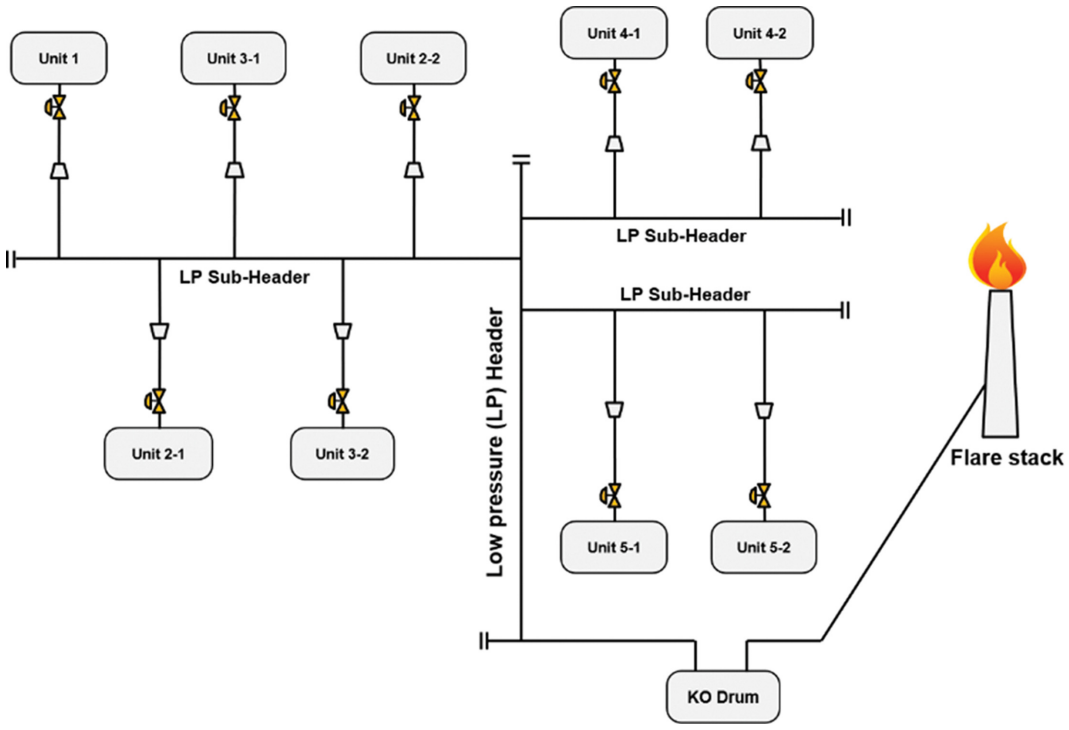

Fig. 3. Schematic of the depressurization system for the LP process.

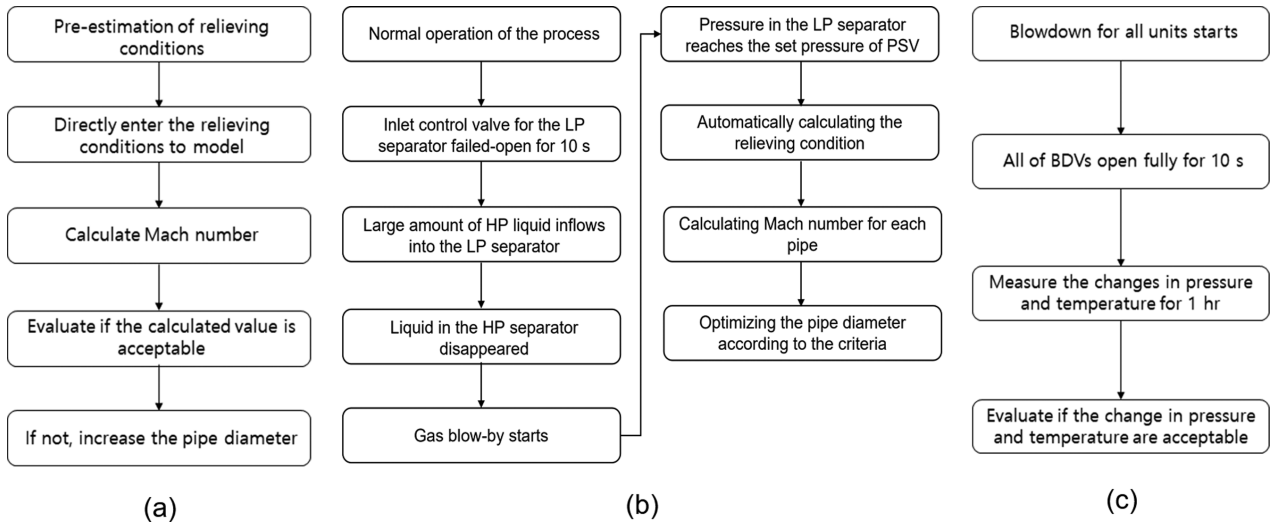

Fig. 4. The flowcharts of each model (a) steady-state model of control fail-open, (b) dynamic model of control fail-open, (c) depressuring system model.

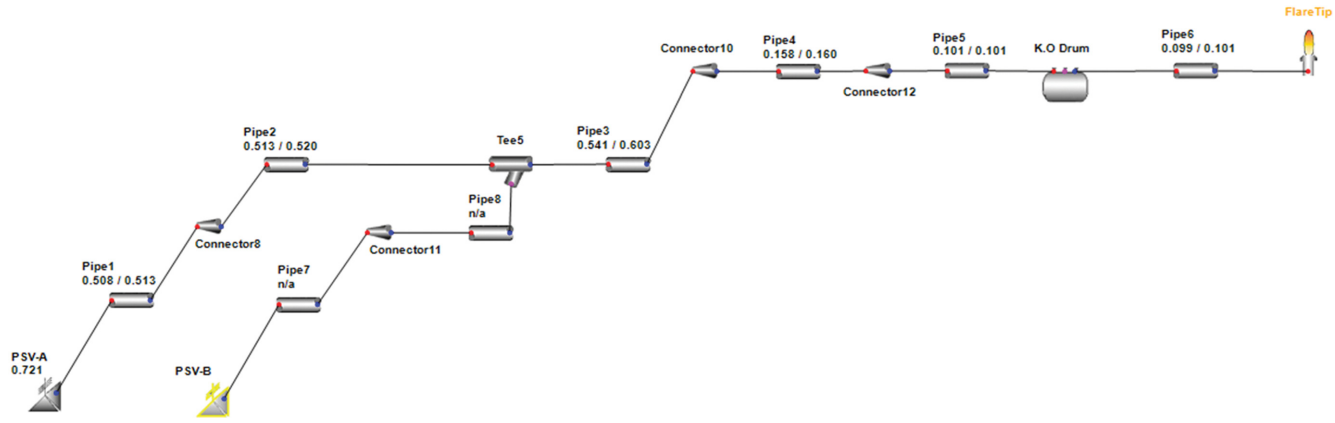

Fig. 5. Steady-state model of inlet control valve fail-open using AFSA.

using the AFSA, it is necessary to estimate the flare loads under the relief scenario, and the estimated relieving conditions, such as relieving temperature, pressure, mole/mass fraction, and flare loads, are directly specified in the source. For this, a design engineer should estimate the expected relevant conditions. However, given that AFSA focuses on flare network system modeling under steady-state conditions, design engineers cannot evaluate the effect of pressure-relieving on the main process and the change in the relieving conditions caused by the change in the main process conditions. In this study, the steady-state model was designed using the data sets of an industrial offshore platform project. Fig. 5 shows the steady-state model for the scenario of inlet control valve fail-open. The steady-state model contains two PSVs, three tailpipes, two main headers, a KO drum, and a flare tip. PSV-A is mainly used in emergencies, and PSV-B is used when PSV-A is under maintenance. The relieving conditions, which are directly entered at each PSV, are in Tables 1 and 2. The design parameters for the PSVs are shown in Table 3. Furthermore, diameters of 10 in. (pipe 1) and 12 in. (pipe 2 and 3) were considered for the tailpipes. The sizes of the main header are 24 in. (pipe 4) and 30 in. (pipe 5).

Table 1. Steady-state relieving conditions

	Relieving conditions
Pressure (bar)	13.47
Temperature (°C)	65.17
Mass flow rate (kg/h)	124,232

Table 2. Mass fraction under relieving conditions

Component	Mass fraction	Component	Mass fraction
CO_2	0.0138	C6*	0.0142
Nitrogen	0.0006	C7*	0.0136
Methane	0.7103	C8*	0.0078
Ethane	0.0776	C9*	0.0033
Propane	0.0563	C10*	0.0012
i-Butane	0.0175	C11*	0.0007
n-Butane	0.0326	H_2S	0.0002
i-Pentane	0.0145	H_2O	0.00165
n-Pentane	0.0145		

Table 3. Design data sheet of PSV

Item	Specification
Set pressure (bar)	11.36
Valve type	Modulating Pilot-operated
Orifice area type	API-T
Inlet pipe diameter (in.)	8
Outlet pipe diameter (in.)	10

Table 4. Feed conditions for the HP separator

Feed conditions	
Pressure (bar)	111
Temperature (°C)	70
Mass flow rate (kg/h)	900,000

2. Dynamic Modeling of Inlet Control Valve Fail-open

Compared with the conventional steady-state model for a flare network system, the dynamic model offers three main advantages, as indicated by the results of our previous study [17]: a) it can analyze the changes in process conditions under the relieving conditions; b) it can help minimize capital costs by optimizing the pipeline size; and c) it considers the uneven distributions of flare loads when multiple PSVs are opened sequentially. In this study, the dynamic model for the inlet control valve fail-open scenario was developed using the gPROMS Process Builder version 1.3, and its schematic is shown in Fig. 6. The feed conditions for the HP separator in the integrated model were obtained from our previous study, as listed in Tables 4 and 5. Additionally, one PSV (PSV-B) was installed for spare. Therefore, it is not used during the emergency relief process. Thus, PSV-B was neglected and not included in the dynamic model. The HP separator shown in Fig. 6 is connected with the reservoir directly and receives high-pressure feed from the subsea region. The high-pressure feed inflows into the HP separator with a pressure of 111 bar, a temperature of 70 °C, and a mass flow rate of 900,000 kg/s. Also, the PCV is operating to maintain the operating pressure. In this study, the liquid level controller for the HP separator was removed to intentionally open the liquid level control valve in order to apply the scenario of control failed-open. We used the Peng-Robinson equation of state to predict the fluid properties because the feed stream components mainly consist of hydrocarbon compounds. The PSVs of the HP separator were removed

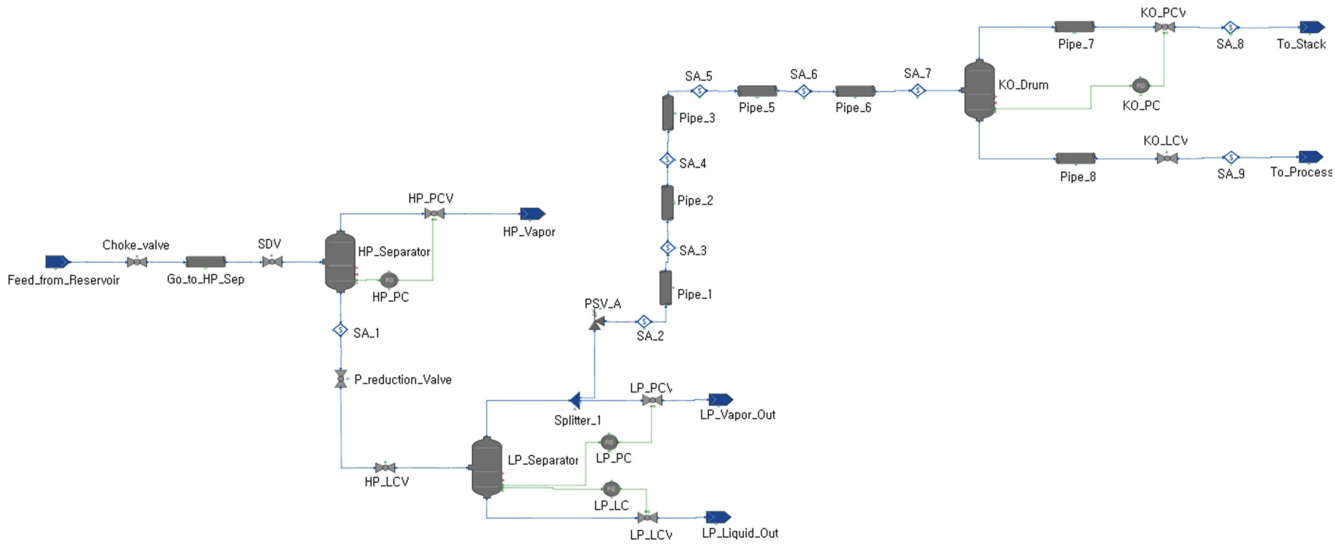

Fig. 6. Dynamic model of inlet control valve fail-open.

Table 5. Mole fraction of the feed stream for the HP separator

Component	Mass fraction	Component	Mass fraction	Component	Mass fraction
CO_2	0.0043	C6*	0.0035	C15*	0.0022
Nitrogen	0.0029	C7*	0.0055	C16*	0.0020
Methane	0.3190	C8*	0.0052	C17*	0.0019
Ethane	0.0273	C9*	0.0031	C18*	0.0013
Propane	0.0137	C10*	0.0036	C19*	0.0020
i-Butane	0.0027	C11*	0.0028	C20+*	0.0022
n-Butane	0.0059	C12*	0.0035	H_2S	0.0002
i-Pentane	0.0027	C13*	0.0030	H_2O	0.5735
n-Pentane	0.0031	C14*	0.0027		

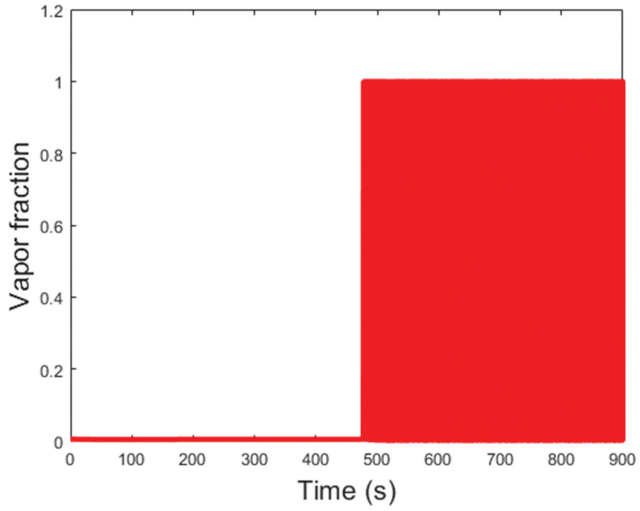

Fig. 7. Fluctuation in the liquid fraction of the feed stream for the LP separator due to the loss of liquid mass at the HP separator.

because the pressure of the HP separator well maintains its set-point value even under the control failed-open scenario.

The computation time for the integrated model is significantly high. A total of 199, 759 s of CPU time is required to complete the calculation for the entire simulation; this is because fluctuations in the liquid fraction of the feed stream for the LP separator lead to a change in the fluid properties based on the fluid phase during the calculation. Furthermore, 281 datasets of calculation results are reported to show the changes in the variables over 1 s. This indicates that 281 calculation iterations, along with the re-initialization procedure, were conducted to acquire the datasets for 1 s of simulation data based on the changes in the fluid phase for all variables. The fluctuations in the liquid fraction of the LP feed stream are shown in Fig. 7. We used an Intel Xeon Silver 4116 CPU with 12 GB RAM and an NVIDIA GeForce GTX 1080Ti GPU for the simulation. The integrated model exhibits the accurate behavior of the main process and the flare network system. For example, we employed two schemes for developing the dynamic model in order to reduce computational time as follows: a) the LP separator was connected with the HP separator until gas blow-by occurred (Fig. 6); b) the gas feed for the LP separator was directly specified to apply the gas blow-by (Fig. 8) by specifying the LP separator's feed conditions with the assumption that the vapor inflowed into the LP separator as the HP separator vapor flowed into the liquid stream. Therefore, the HP separator is not shown in Fig. 8. In comparison, the calculated Mach number in both cases shows a significant difference. The dynamic model has a maximum value of 0.23, whereas the after-gas blow-by model has a maximum value of 0.7, as shown in Fig. 9. Here, the integrated model (Fig. 9(a)) represents that the LP separator is connected to the HP separator, and after gas blow-by model (Fig. 9(b)) represents that the feed conditions of the LP separator are directly specified as the vapor conditions of HP separator when the gas blow-by occurs. Since a larger Mach number causes a larger diameter of the pipe at the process design step, the overall capital cost increases when the steady-state model is used for designing the flare network system. Given that, in the actual process, the HP separator receives the HP feed through a riser from the subsea when the event occurs, a small amount of liquid from the HP separator is still discharged with the HP vapor via the fully opened valve. Thus, the fluctuations in the liquid fraction of the feed stream for the LP separator were more realistic. Also, the fluctuation of the liquid fraction can lead to less vapor in the pipe, representing that the vapor and liquid are inflowing into the LP separator. Therefore, the calculated Mach number in 'after gas blow-by' is greater than the integrated model because the feed conditions for this model are considered as vapor only. Hence, we can obtain more realistic results and optimize the pipeline size via dynamic simulations, which could lead to a reduction in the capital costs.

3. Depressurization Modeling

Fig. 10 presents the flowsheet of the depressurization system,

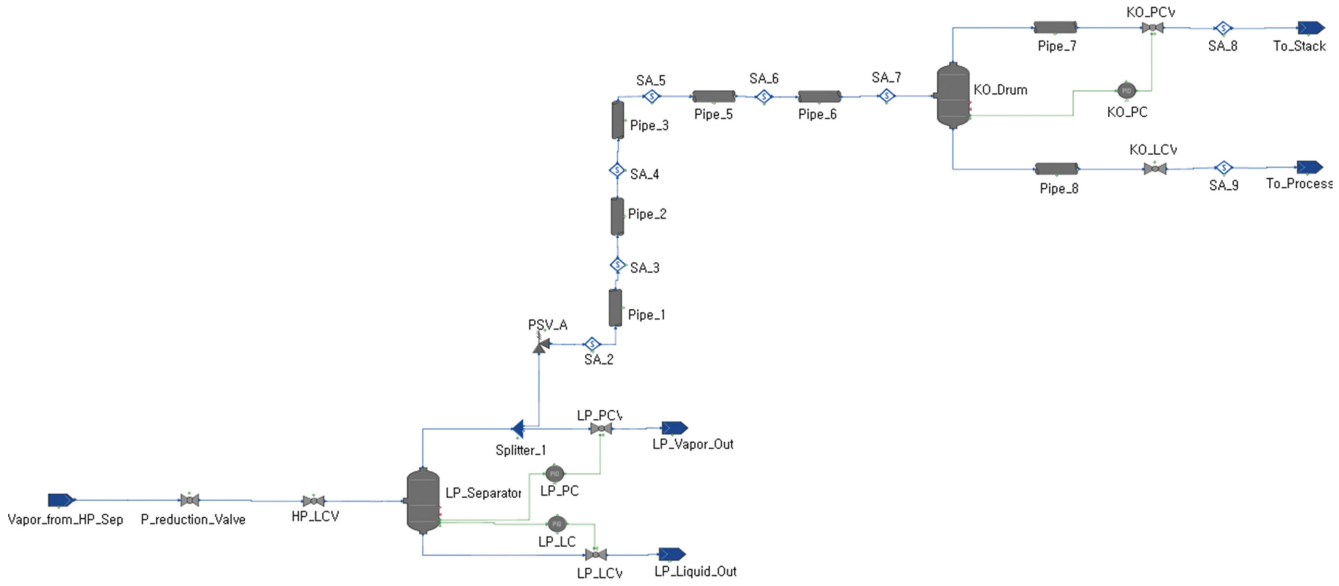

Fig. 8. Dynamic model of the "after gas blow-by" scenario.

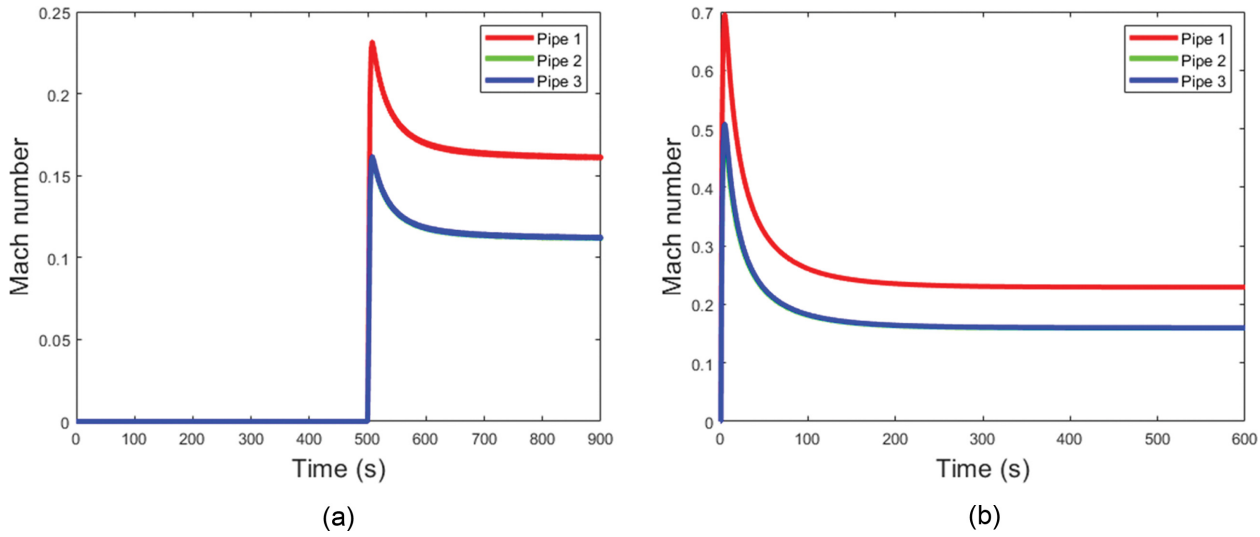

Fig. 9. Comparison of the maximum Ma between the (a) integrated and (b) after gas blow-by models.

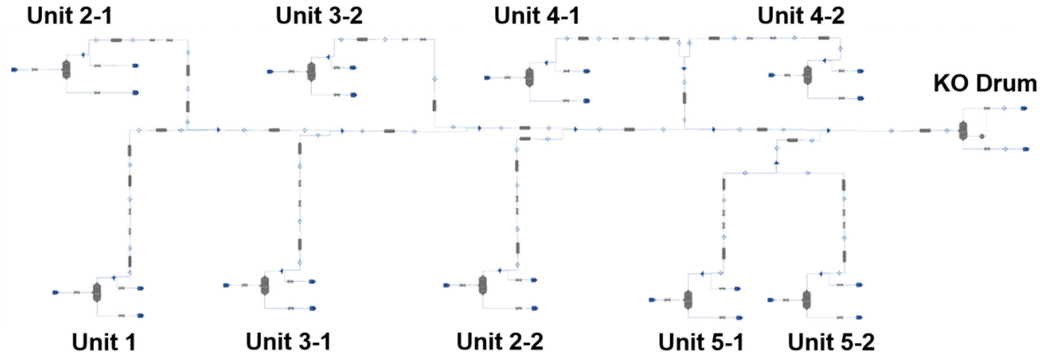

Fig. 10. Flowsheet of the depressurization system for the LP process.

developed using gPROMS Process Builder version 1.3. Each unit was connected to the LP header line through the tailpipes. The optimal method of reducing the pressure of each unit involves rapid release of the HP gas from the over-pressurized units. Therefore, the gas depressurization process is considered in this study. Additionally, we assumed that the pressure and temperature of each unit are within the design limits, which are the maximum allowable conditions for the units, to evaluate the suitability of the designed depressurization system under severe conditions. To evaluate the acceptability of the process design, the regulations from API Standard 521 were adopted: a) reduction of pressure by 50% of the design pressure within 15 min or b) depressuring to a pressure of 100 psig (8 bar) within 15 min. The conditions under which depressurization is commenced are shown in Table 6.

Table 6. Conditions of the LP process units when the depressuring process commences

	Pressure (bar)	Temperature (°C)
Unit 1	25.15	65.55
Unit 2-1	11.36	83.95
Unit 2-2	11.36	83.95
Unit 3-1	25.15	66.85
Unit 3-2	25.15	66.85
Unit 4-1	11.36	84.85
Unit 4-2	11.36	84.85
Unit 5-1	11.36	70.85
Unit 5-2	11.62	70.85

RESULTS AND DISCUSSIONS

The results of the dynamic model for the scenarios, namely "inlet control valve fail-open" and "depressuring system," are presented in this section. First, the dynamic behaviors of the HP separator and the LP separator under the inlet control valve fail-open scenario were analyzed. Secondly, the changes in the relieving condition at the PSV were analyzed. The pipeline size for the flare network system was optimized based on API Standard 521. After obtaining the results for the inlet control valve fail-open scenario, the results for the non-fire depressuring scenario were analyzed.

1. Dynamic Changes for the HP Separator

The failure of the inlet control valve occurs at a simulation time of 300 s to ensure process stability before commencing the event,

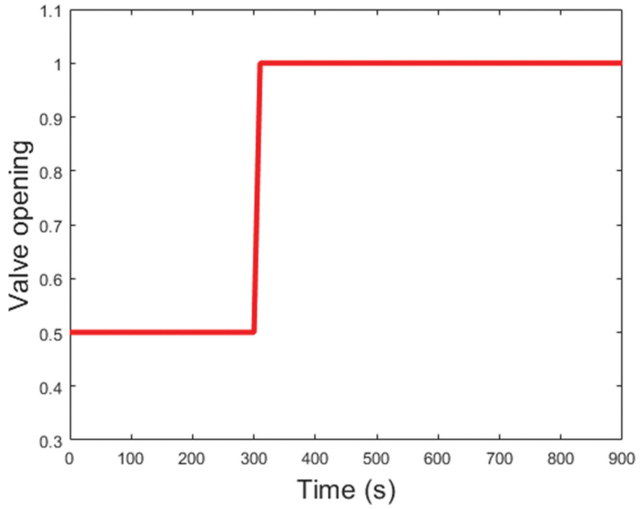

Fig. 11. Inlet control valve fail-open procedure.

as shown in Fig. 11. Therefore, the HP separator maintains its operating pressure (13.13 bar) and liquid level fraction (0.36) until the failure of the inlet control valve for the LP separator, as shown in Fig. 12(a) and Fig. 12(b). Given that the pressure of the HP separator is regulated by the pressure controller, it recovers its set-point quickly when the inlet control valve for the LP separator fails. Once gas blow-by occurs, the pressure of the HP separator abruptly decreases by 13.123 bar owing to the HP vapor release, and it recovers its set-point value again. The liquid level fraction of the HP separator begins to decrease immediately when the event occurs and eventually reaches zero at 477 s. Given that, under the gas blow-by scenario, the separated liquid phase of the feed stream for the HP separator is discharged immediately, the liquid level remains at zero.

2. Dynamic Changes for the LP Separator

Similar to the HP separator, the LP separator maintains its set-point values of liquid level fraction and pressure at 0.547 and 7.2 bar, respectively, until the event commences, as shown in Figs. 13(a) and 13(b). However, the pressure of the LP separator increased gradually once the event commenced (300 s), although the pressure control valve was fully open, as shown in Fig. 14. This represents that the pressure control valve cannot regulate the pressure of the LP separator due to its insufficient size. Owing to the HP vapor inlet from the HP separator (gas blow-by) into the LP separator, the pressure in the LP separator increases abruptly. This implies that the pressure control valve is unable to regulate the pressure when a gas blow-by event occurs. Even though the HP liquid inflows into the LP separator when the inlet control valve fails, the rapid increase in the pressure of the LP separator can be prevented by extracting a large amount of liquid by operating the liquid level controller. However, when the HP vapor inflows into the LP separator, the pressure of the LP separator is directly affected by the inflowing vapor conditions and rapidly increases up to 11.47 bar, which is the set-point pressure of the PSV. Once the PSV opens at 503 s, the pressure remains constant. The liquid level fraction slightly increases from its set-point value of 0.547 because of the large amount of liquid inlet from the HP separator as the event commences, but it recovers its set-point value quickly by operating the liquid level controller. When gas blow-by was initialized, the liquid level of the LP separator decreased and was returned to its set-point value by adjusting the liquid level control valve. The properties of the inlet and outlet streams of the LP separator at normal operation and gas blowby are shown in Table 7. Considering that it takes a short time to open the PSV when the inlet control valve fails, the normal operation of the outlet controllers of the LP separator is acceptable during this event. Additionally, given that some time is required for decision-making and applying the procedure, it is difficult to recognize and stop the operation within this short time interval.

3. Dynamic behavior of PSV

Once the PSV opens, it remains open for the remaining duration of the simulation. Initially, the PSV is closed, but as the pressure of the LP separator increases, the PSV begins to open to prevent overpressure in the LP separator, as illustrated in Fig. 15. As we assume that the HP and LP separators are operating with respect

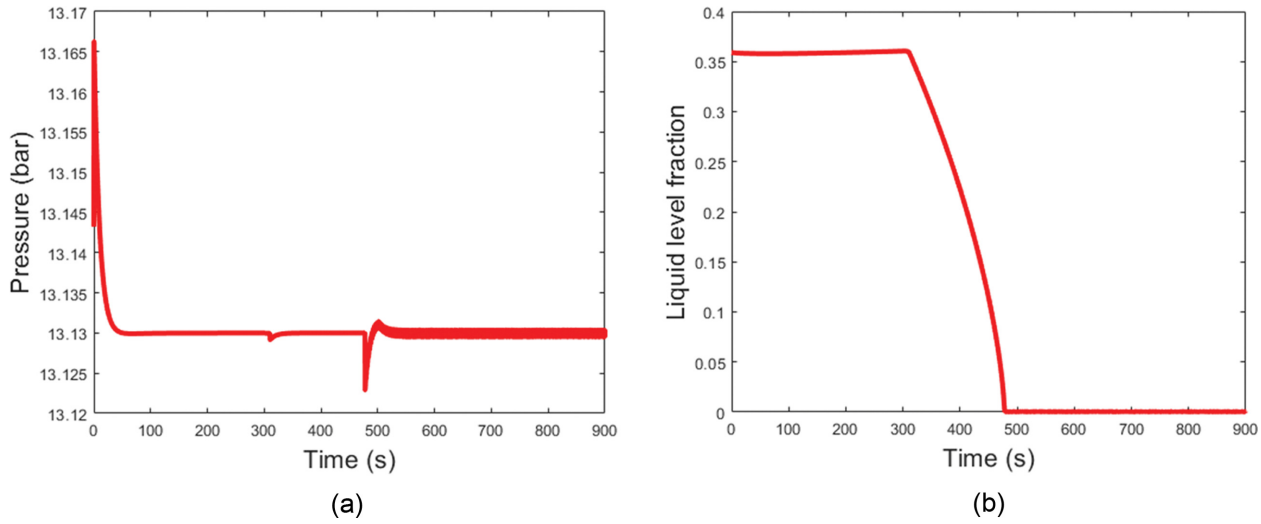

Fig. 12. Dynamic changes in operating conditions of HP separator.

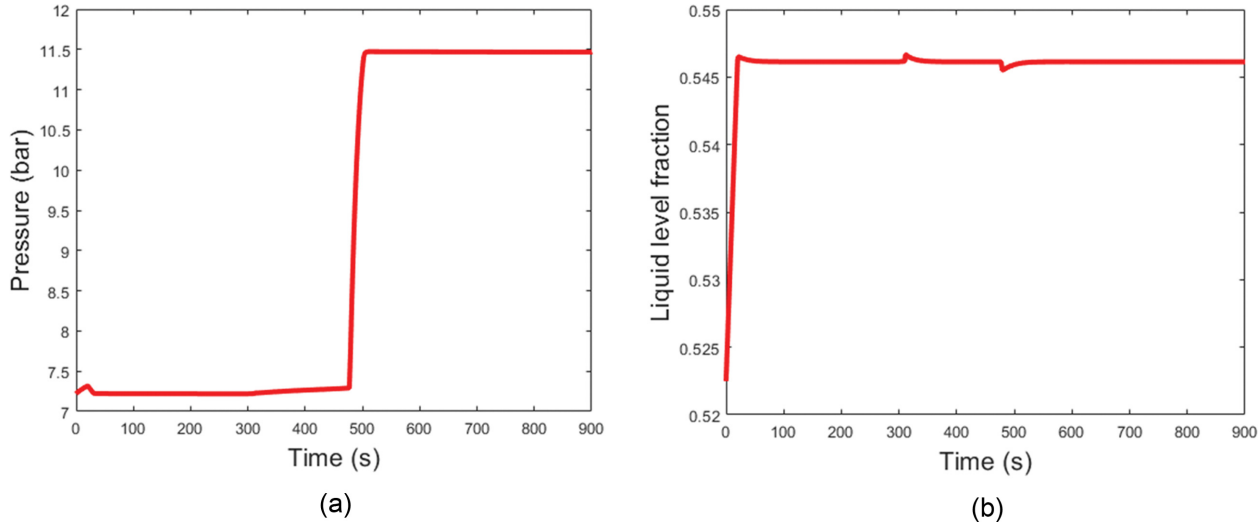

Fig. 13. Dynamic changes in the conditions of the LP separator.

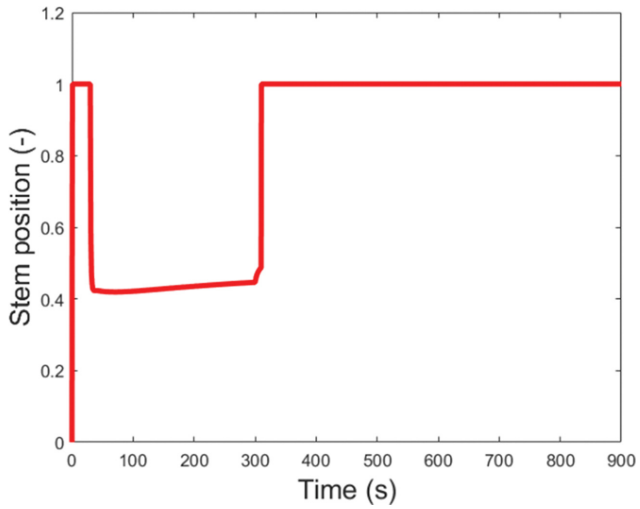

Fig. 14. Stem position of LP-PCV.

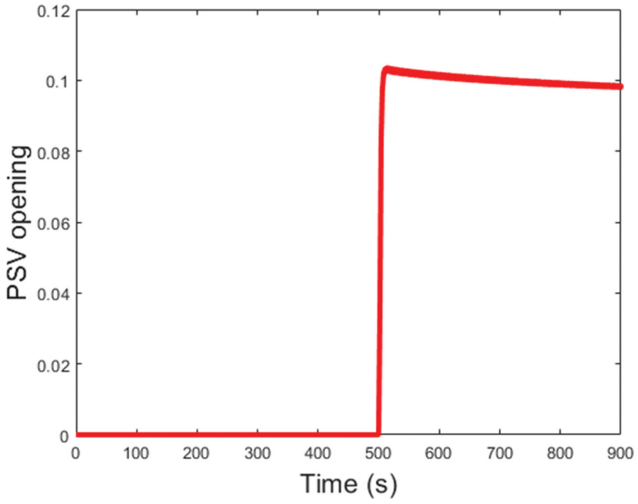

Fig. 15. Stem position of the PSV.

to the controllers (i.e., PCV of the LP and HP separator and LCV of the LP separator) except the LCV of the HP separator (failed-open), the HP vapor from the HP separator continuously flows into the LP separator. Hence, the PSV remains open with a stem position of 0.098. The stem position of the PSV had a maximum value of 0.104 at 517 s. Similar to the stem position of the PSV, the mass flow rate has a maximum value of 3.57 kg/s at 513 s, as shown in Fig. 16(a). The backpressure of the PSV increases gradually from 1 bar, reaching a maximum value of 1.506 bar, which is below the regulations of API Standard 521. Given that the normal operation of the KO drum is approximately 1 bar, the initial backpressure is considered to be 1 bar [28,29]. The backpressure main-

Table 7. Inlet and outlet conditions change of the LP separator

		Pressure (bar)	Temperature (°C)	Mass flow rate (kg/s)
Normal operation	LP in	7.22	77.30	88.73
	LP vapor out	7.22	77.30	0.43
	LP liquid out	7.22	77.30	86.73
Gas blow-by	LP vapor in	11.47	66.27	112.38
	LP liquid in	11.47	66.27	13.98
	LP vapor out	11.47	66.27	5.86
	LP liquid out	11.47	66.27	66.68

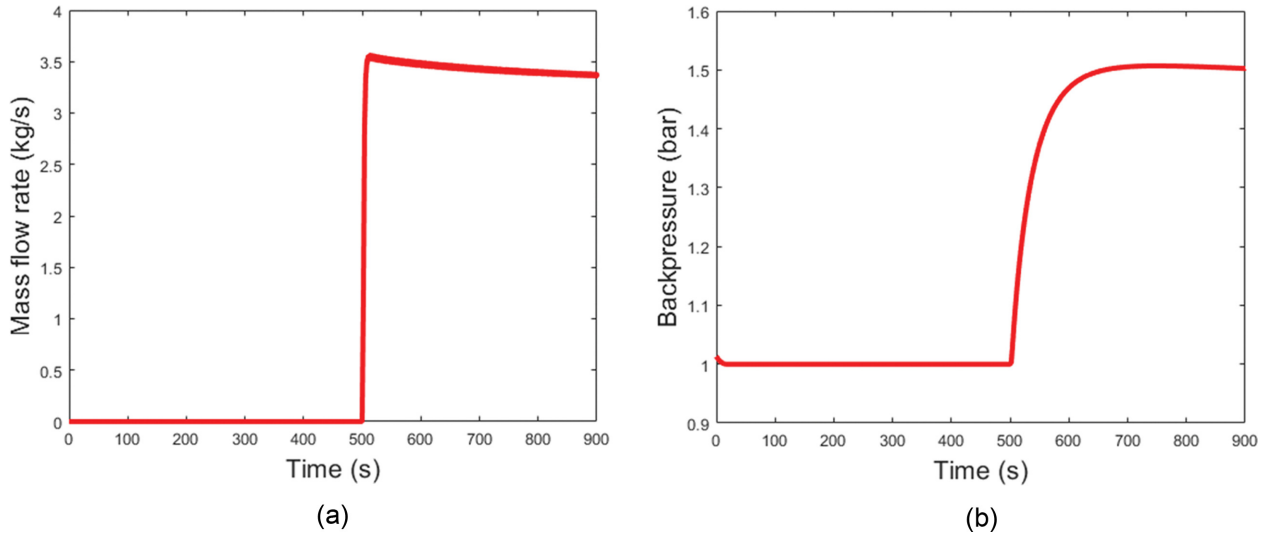

Fig. 16. Mass flow rate of flare loads and back pressure of the PSV.

tained its value after reaching the maximum value of 1.506 bar, as shown in Fig. 16(b).

4. Mach Number Calculation and Pipe Size Optimization

Based on API Standard 521 and the NORSOK Standard, the Mach number (Ma) of the pipe for a flare network system should not exceed certain limitations; thus, it should be less than 0.7 and 0.5 for the tailpipes and headers, respectively. Additionally, it is recommended that the maximum backpressure should be less than 50% of the set pressure of the PSV when the modulating pilot-operated PSV is used. In this study, the backpressure was automatically calculated using the dynamic model. However, a user-defined function must be used to calculate Ma. Hence, Eq. (1) was used to calculate Ma, as described in API Standard 521:

$$Ma = 3.23\times10^{-5}\left(\frac{\dot{m}}{P\times D^2}\right)\left(\frac{Z\times T}{M_w}\right)^{0.5} \quad (1)$$

where $\dot{m}$ denotes the mass flow rate in the pipe (kg/h), P denotes the pipe outlet pressure (kPa), D denotes the diameter of the pipe outlet (m), Z denotes the compressibility factor, T denotes the temperature of the pipe outlet (K), and Mw denotes the average molecular weight of the fluid in the pipe. Note that the units of all the variables are in SI units. If the USC unit is applied, then the constant of 3.23×10^{-5} should be changed to 1.702×10^{-5}.

The calculated Ma of each pipe in the steady-state and dynamic models are shown in Fig. 17 and in Table 8. The Ma for the headers was not considered in this study because this scenario is not the governing case for the LP headers. The governing scenario for the LP header is the scenario of "HP separator outlet blockage," as described in our previous study [17]. Given that the Ma in the dynamic model changes according to the relieving conditions, such as the mass flow rate of the flare loads and back pressure, the maximum value of the calculated Ma is used for comparison with the steady-state model. The calculated Ma for all pipes in the steady-state model is higher than that calculated via the dynamic model. Furthermore, for pipe 1, the value exceeds that prescribed by API Standard 521 (less than 0.7 for tailpipes). To satisfy the requirement in the steady-state model, the diameter of pipe 1 must be increased to 12 in. On the other hand, the results from the dynamic simulations show that the maximum Ma of each pipe is significantly small. Therefore, the diameter of the pipes can be reduced via optimization. The main reason for the difference in the calculated Mach number in those models is that the steady-state model cannot consider the changes of the process conditions over time under various events. Considering that the relieving conditions are strongly affected by the process conditions, it is inappropriate to use only predefined relieving conditions at steady-state condition. Therefore, exact estimation of the relieving conditions based on the process conditions is crucial to calculate the Mach number and decide the pipe size. Thus, the automatically estimated relieving conditions as the event proceeds cause the difference in the calculated

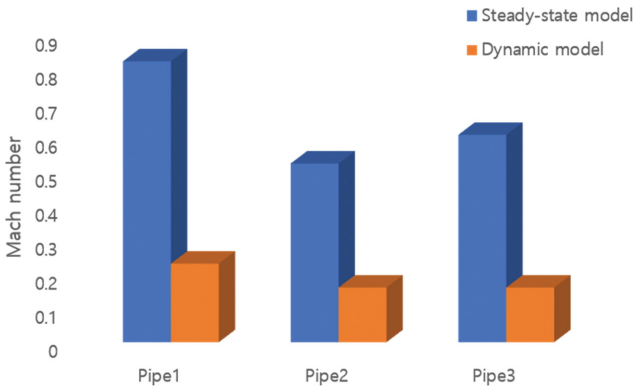

Fig. 17. Comparison of Ma calculated via the steady-state and dynamic models.

Table 8. Calculated Ma for the steady-state and dynamic models

	Pipe 1	Pipe 2	Pipe 3
Steady-state model	0.82	0.52	0.61
Dynamic model (max. value)	0.23	0.16	0.16

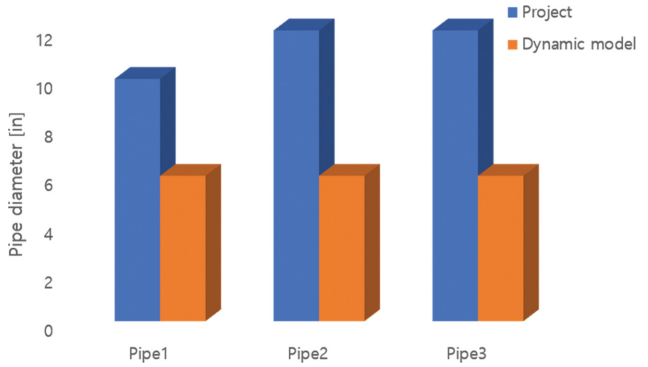

Fig. 18. Comparison of pipe diameters calculated from the project data and the dynamic model.

Table 9. Calculated diameters for each pipe

Pipe number	Diameter (in.)	Selected diameter (in.)
Pipe 1	5.73	6
Pipe 2	5.74	6
Pipe 3	5.75	6

Mach number in steady-state and dynamic models.

Subsequently, the pipeline size is optimized using Eq. (1) considering the occurrence of gas blow-by. Furthermore, Ma in Eq. (1) is set to a maximum value of 0.7, and the pipe diameter remains a dependent variable. Thus, Eq. (2) is derived from Eq. (1):

$$D = \left[4.61\times10^{-5}\left(\frac{\dot{m}}{P}\right)\left(\frac{Z\times T}{M_w}\right)^{0.5}\right]^{0.5} \quad (2)$$

The diameter of each pipe calculated from Eq. (2) was compared with the data of the industrial project; this comparison is presented in Fig. 18 and Table 9. Typically, pipe sizes are standardized. Therefore, we selected the pipe diameter according to the nominal pipe sizes offered by Dacapo Stainless Steel. The optimization results reveal that the pipe diameter can be significantly reduced, while also satisfying the constraints. Specifically, the diameters of pipes 1, 2, and 3 can be reduced to 6 in. This implies a maximum reduction of 50% in size. Specifically, Ma for each pipe after optimization is shown in Fig. 19. The regulations on the backpressure related to the type of PSV also need to be satisfied. After optimizing the pipeline size, the backpressure is 1.65 bar, as illustrated in Fig. 20(a), which satisfies the regulations of API Standard 521 and the NORSOK Standard. Among all the tailpipes, the maximum value of ρv^2 was found at pipe 3 (i.e., 41,642 kg/(m s^2)), as shown in Fig. 20(b); this is below the constraint of 200,000 kg/(m s^2).

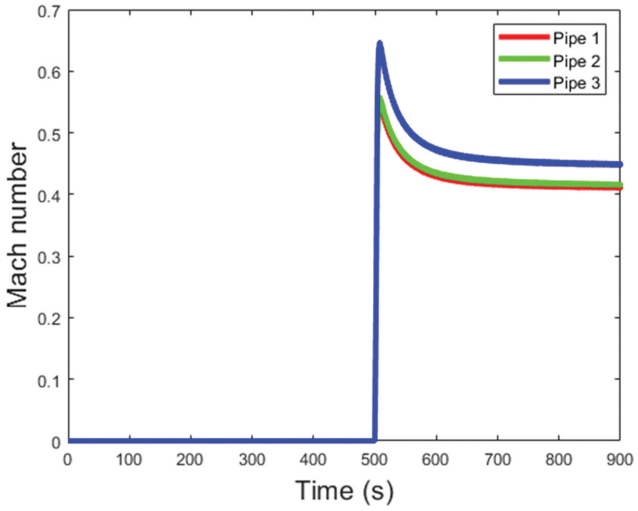

Fig. 19. Ma for each pipe after optimization.

5. Analysis of Depressurization Process

The depressuring rate of each unit installed in the LP system is shown in Fig. 21. The LP system units mainly consist of two species, i.e., the LP and HP units; Fig. 21(a) shows the depressuring rate for the LP units, while Fig. 21(b) shows the one for the HP

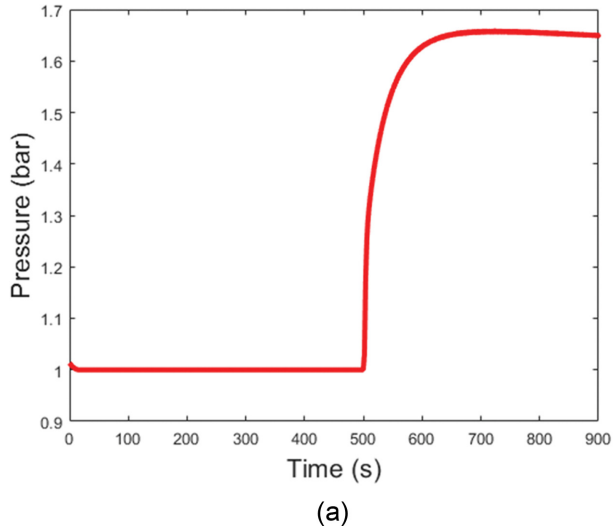

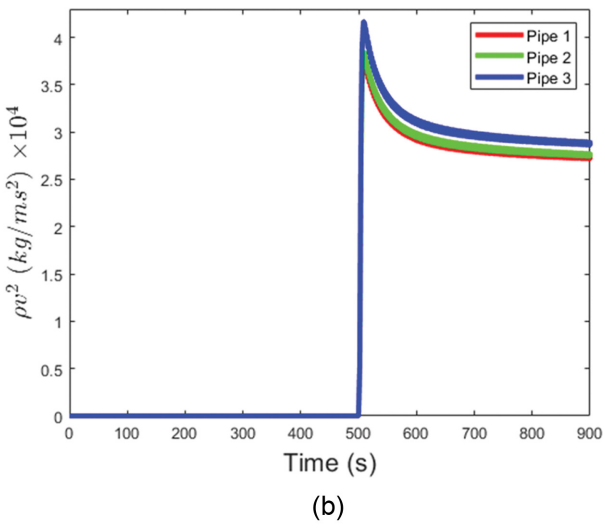

Fig. 20. (a) Backpressure and (b) ρv^2 for each pipe after optimization.

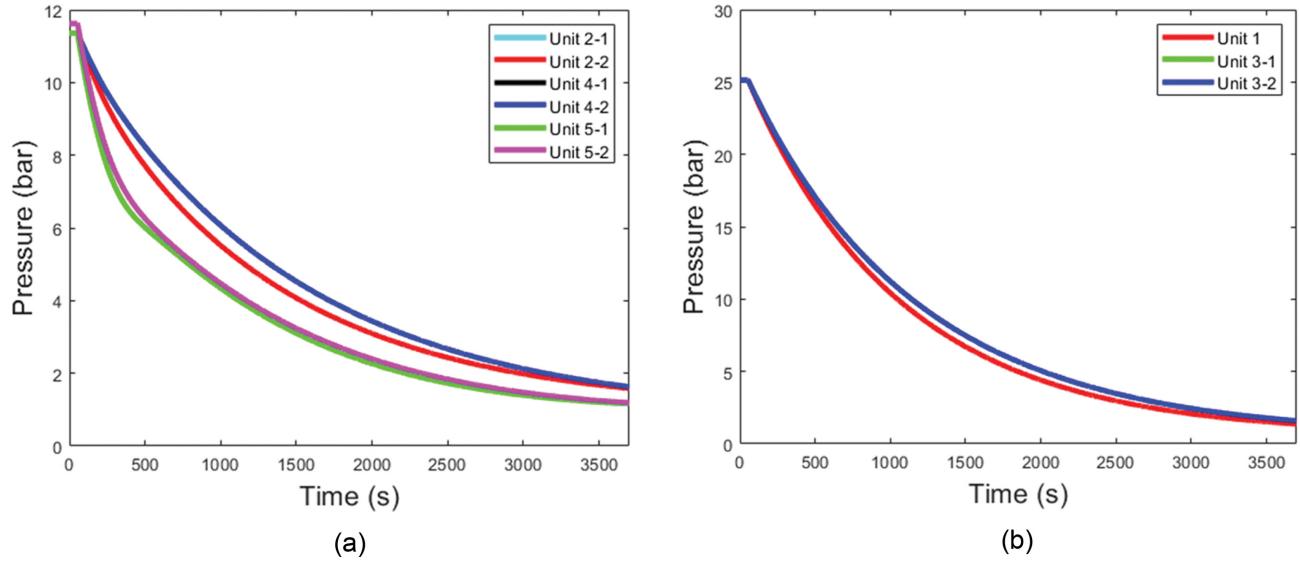

Fig. 21. Depressuring rate for (a) LP units and (b) HP units.

units. In this study, the depressuring process commenced at 50 s, and all the blowdown valves in the LP process began to open over 10 s. The total simulation time for the depressuring process was 3,700 s, which included the initial 50 s and the blowdown valve opening time of 10 s. The depressuring rate for each unit over 15 min is listed in Table 10. The results show that all the HP units in the LP process satisfy the regulations of API Standard 521. Specifically, the pressure of unit 1 decreases from 25.15 bar to 10.81 bar over 15 min (57% depressuring). Similarly, the pressures of the HP units in the LP process, i.e., units 3-1 and 3-2, decreased by 54% over 15 min. Therefore, the depressuring rate for HP units in the LP process did not violate the regulations. By contrast, the LP units, i.e., units 4-1 and 4-2, in the LP process did not satisfy the 50% depressuring rate. However, they satisfied the condition of depres-

Table 10. Depressuring rate for each unit in the LP process

	Initial pressure (bar)	Pressure at 15 min (bar)	Depressuring rate (%)
Unit 1	25.15	10.81	57
Unit 2-1	11.36	5.66	50
Unit 2-2	11.36	5.66	50
Unit 3-1	25.15	11.60	54
Unit 3-2	25.15	11.60	54
Unit 4-1	11.36	6.21	45
Unit 4-2	11.36	6.21	45
Unit 5-1	11.36	4.46	61
Unit 5-2	11.62	4.59	60

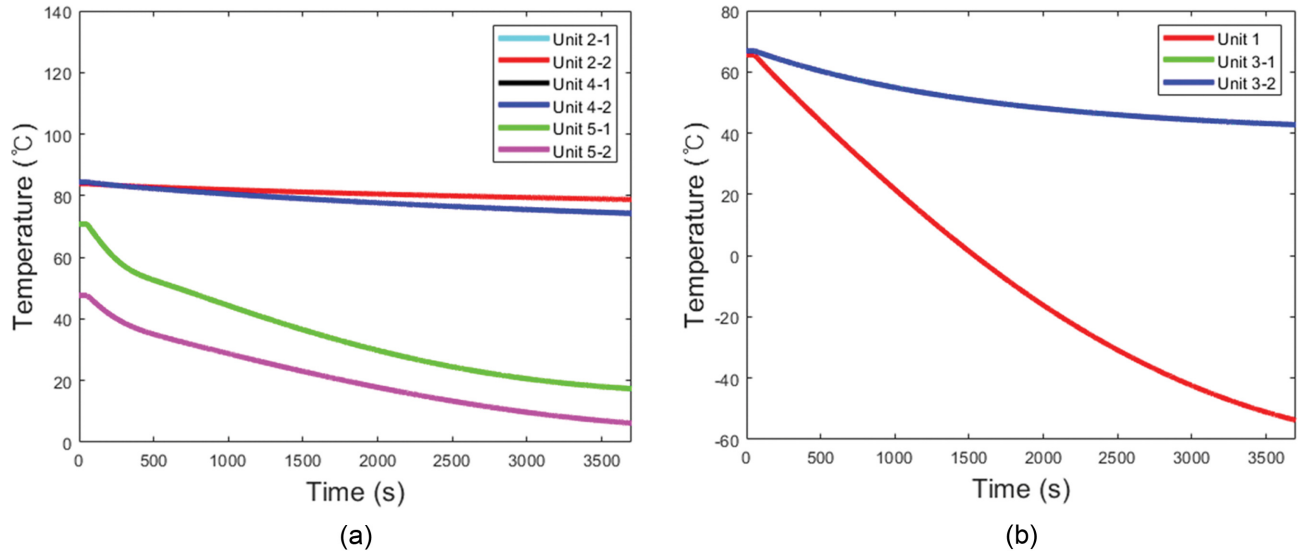

Fig. 22. Temperature changes in (a) LP units and (b) HP units.

suring up to 100 psig (8 bar). Specifically, the pressures of units 2-1 and 2-2 decreased from 11.36 bar to 5.66 bar (50% depressuring), whereas those of units 4-1 and 4-2 decreased from 11.36 bar to 6.21 bar (45% depressuring). Therefore, considering that the pressure decreases to less than 100 psig (8 bar), the size of the LP unit's blowdown valves is sufficient to satisfy the requirements. The temperature changes in the LP and HP units are shown in Fig. 22(a) and 22(b), respectively. The minimum design temperature of the LP and HP units is −30 °C, as per the industrial project datasheet. Therefore, with the exception of unit 1, all the units are safe from failure. The temperature of unit 1 undergoes a rapid decline (decreases to −53.7 °C), as compared to units 3-1 and 3-2. However, the initial temperature and pressure of the depressuring process are similar. This significant decrease in the temperature of unit 1 is mainly due to the small vessel volume and relatively large blowdown size of the valve with respect to the vessel volume. Therefore, unit 1 can fail if the non-fire depressuring process is conducted. Thus, the blowdown valve should be re-sized to ensure that it is smaller than its current size, in order to prevent accidents due to the brittleness of the vessel, caused by the significantly low temperatures. Otherwise, a slow depressuring strategy is required.

CONCLUSIONS

Flare network systems are usually designed based on steady-state conditions. However, the steady-state-based design can lead to an overestimation of the size of pipelines. This, in turn, increases capital costs and limits the availability of space on offshore platforms. Therefore, to minimize capital costs and maximize spatial availability, optimizing pipeline sizes via dynamic analyses of the flare network system is necessary. Thus, in this study, the flare network system of an offshore platform was dynamically analyzed under two separate scenarios: inlet control valve fail-open and depressuring system.

The HP model developed in our previous study is integrated with an LP separator to obtain more realistic results under the inlet control valve fail-open scenario, as compared to the results obtained using the LP separator alone. Subsequently, the results from the dynamic model were compared with those of the steady-state model, and the pipeline size was optimized.

The results reveal that, with regard to the offshore industrial project, the size of pipe 1, which is connected to the PSV, is inappropriate under the steady-state-based model, because the Ma exceeds the regulations set by API Standard 521. By contrast, the dynamic model shows that the maximum Ma of each pipe is lower than that set by API Standard 521. Therefore, the size of the pipeline can be optimized, leading to a decrease in the capital cost and a maximization of spatial availability on the offshore platform. The optimization results reveal that the pipeline size can be reduced by a maximum of 50%.

Additionally, a dynamic analysis of the depressuring system for the LP process on the offshore platform was performed, considering API Standard 521 as a criterion, in order to evaluate the acceptability of the design specification for units and the size of the blowdown valve. The results indicate that all the LP process units satisfy API Standard 521, i.e., depressuring up to 50% of design pressure or 100 psig (8 bar). However, the temperature of unit 1, among the HP units, decreases rapidly and is considerably low, although the initial conditions in the depressuring process are similar to those of units 3-1 and 3-2. This is due to the relatively large blowdown valve size with respect to the vessel volume. The extremely low temperature during the non-fire depressuring process can lead to vessel failure. This, in turn, leads to the leakage of the volatile hydrocarbon liquid. Therefore, slow depressuring should be applied to unit 1 when a non-fire depressuring process is conducted.

A dynamic analysis of flare network systems produces more realistic results than a steady-state analysis by integrating the process with the flare network system. Therefore, overestimation of the capital costs can be avoided, which, in turn, maximizes profits for the engineering and construction industries. Furthermore, this approach allows engineers to investigate the operating condition more thoroughly at the design stage of the process so that any unexpected accident during operation can be avoided in advance.

ACKNOWLEDGEMENT

This research was supported by INHA UNIVERSITY Research Grant.

REFERENCES

1. Y. Cho, S. Kwon and S. Hwang, *Korean J. Chem. Eng.*, **35**, 20 (2018).
2. Standard, A. P. I, *Pressure-relieving and depressuring systems* (2014).
3. T. Baalisampang, R. Abbassi, V. Garaniya, F. Khan and M. Dadashzadeh, *Fire Safety J.*, **92**, 42 (2017).
4. L. W. D. Cullen, *Drilling Contractor*, **49**, 4 (1993).
5. S. Kabir, M. Taleb-Berrouane and Y. Papadopoulos, *Energy Sources, Part A: Recovery, Utilization, and Environmental Effects*, 1 (2019).
6. M. T. Berrouane and Z. Lounis, *J. Chem. Technol. Metall.*, **51**, 229 (2016).
7. S. M. Deyab, M. Taleb-Berrouane, F. Khan and M. Yang, *Process Saf. Environ. Prot.*, **113**, 220 (2018).
8. K. Park, D. Shin and W. Won, *Korean J. Chem. Eng.*, **35**, 1053 (2018).
9. J. Smith, H. Al-Hameedi, R. Jackson and A. Suo-Antilla, *Int. J. Petrochem. Res.*, **2**, 175 (2018).
10. X. Wu, C. J. Li, W. L. Jia and J. C. Mu, *Int. Pet. Technol. Conf.*, **5**, 2843 (2019).
11. E. Yazdani, J. Asadi, Y. H. Dehaghani and P. Kazempoor, *J. Nat. Gas Sci. Eng.*, **84**, 103627 (2020).
12. Z. Hamidzadeh, S. Sattari, M. Soltanieh and A. Vatani, *Energy*, **203**, 117815 (2020).
13. N. Tahouni, M. Gholami and M. H. Panjeshahi, *Energy*, **111**, 82 (2016).
14. J. Tovar-Facio, F. Eljack, J. M. Ponce-Ortega and M. M. El-Halwagi, *ACS Sustainable Chem. Eng.*, **5**, 675 (2017).
15. R. Wasnik, H. Singh, F. R. Kamal and O. H. Takieddine, *Abu Dhabi Int. Pet. Exhib. Conf*, **2**, 787 (2018).
16. Standard, NORSOK, *Process System Design* (2014).
17. Y. P. Jo, Y. Cho and S. Hwang, *Process Saf. Environ. Prot.*, **134**, 260 (2020).
18. M. Davoudi, A. Aleghafouri and A. Safadoost, *J. Nat. Gas Sci. Eng.*, **21**, 221 (2014).

19. L. L. Pemii, K. K. Dagde and T. O. Goodhead, *Adv. Chem. Eng. Sci.*, **10**, 297 (2020).
20. U. V. Shenoy, *Chem. Eng. Res. Des.*, **89**, 2686 (2011).
21. A. X. O. Somozas, R. P. Nielsen, M. Maschietti and A. Andreasen, *J. Loss Prev. Process Ind.*, **67**, 104211 (2020).
22. U. Shafiq, A. M. Shariff, M. Babar, B. Azeem, A. Ali and M. A. Bustam, *Process Saf. Environ. Prot.*, **133**, 104 (2020).
23. U. Shafiq, A. M. Shariff, M. Babar, B. Azeem, A. Ali and A. Bustam, *J. Loss Prev. Process Ind.*, **64**, 104073 (2020).
24. A. Surmi, *Int. Pet. Technol. Conf.*, **4**, 2305 (2019).
25. A. A. M. Jalil, M. F. M. Isa, K. Rostani, N. A. Othman, A. M. Shariff, K. K. Lau, B. Partoon and W. H. Tay, *SPE Annu. Tech. Conf. Exhib.*, **7**, 4877 (2019).
26. F. H. Rahman, F. M. Isa, R. S. Salihuddin, M. Jalani, F. Karim and W. M. W. Hashim, *Offshore Technology Conference Asia*, **3**, 1702 (2018).
27. K. Ebrahimi, S. R. Mofrad, B. Millet, K. Kirkpatrick and G. Miller, *Proc. ASME Pressure Vessels Piping Conf.*, **3A** (2018).
28. O. Zadakbar, F. Khan and S. Imtiaz, *Risk Analysis*, **35**, 713 (2015).
29. R. Hernandez-Suarez, H. Puebla and R. Aguilar-Lopez, *Ind. Eng. Chem. Res.*, **46**, 7008 (2017).